Nonlinear optical properties of perovskite $YMnO_3$ studied by real-space recursion method

Xiangang Wan, Jinming Dong, Meichun Qian, and Weiyi Zhang
National Laboratory of Solid State Microstructures and Department of Physics, Nanjing University, Nanjing 210093, People's Republic of China
(Received 7 September 1999)

New types of second-order nonlinear optical properties of hexagonal $YMnO_3$ have been studied, caused by the coexistence of the noncentrosymmetric ferroelectric ordering of charges and the centrosymmetric spin ordering below its Neel temperature T_N. Using time-dependent perturbation theory and the Green's function method, we have derived an expression for the nonlinear optical susceptibility in terms of the real-space Green's function. Then, based upon the multiband Hubbard Hamiltonian and the unrestricted Hartree-Fock approximation, the real-space recursion method has been used to calculate the electric structure of $YMnO_3$ below T_N, and its nonlinear optical susceptibility. The calculated results are very consistent with the experimental observation, and clearly show different contributions to the nonlinear optical response from the Mn e_g and Op bands in $YMnO_3$.

I. INTRODUCTION

The discovery of colossal magnetoresistance in mixed-valent manganese perovskites, such as $La_{1-x}Ca_xMnO_3$, has attracted renewed interest in these doped rare-earth manganese oxides because of their potential technological applications and similarity to the cuprate superconductors.[1] Usually, the rare-earth and yttrium manganites $RMnO_3$ have two structural phases[2]: a hexagonal phase for $R=$ Ho, Er, Tm, Yb, Lu or Y, which has a small ionic radius; and an orthorhombic phase for $R=$ La, Ce, Pr, Nd, Sm, Eu, Gd, Tb or Dy, which has a greater ionic radius. Although magnetic ordering can occur in both hexagonal and orthorhombic manganites, ferroelectric ordering occurs only in hexagonal ones having noncentrosymmetric symmetries (the $P6_3cm$ space group).

Therefore, hexagonal yttrium and rare-earth manganites comprise an interesting class of materials known as ferroelectromagnets, in which ferroelectric and magnetic orders coexist at low temperatures. Indeed, the coupling phenomenon between the ferroelectric and magnetic orders was recently observed in $YMnO_3$,[3] which displays a ferroelectric $T_C \approx 914$ K, but a rather low antiferromagnetic $T_N \approx 80$ K. This coupling can lead to a so-called magnetoelectric effect, with an interesting potential use in devices, where the dielectric (magnetic) properties may be changed by the onset of a magnetic (electric) transition or by application of an external magnetic (electric) field. Physically, the more important part of optical nonlinearity comes from the electric-dipole mechanism, including the magnetization-induced second-harmonic generation (SHG) of electric-dipole character.[4–8] As is well known, the second-order optical susceptibility can exist only in a material with a broken space-inversion symmetry. However, a quite different mechanism of electric-dipole nonlinearity was found in the magnetoelectric crystal Cr_2O_3, with a centrosymmetric charge distribution but a noncentrosymmetric antiferromagnetic spin order.[4] Hexagonal $YMnO_3$ has a noncentrosymmetric ferroelectric ordering of charges and a centrosymmetric spin ordering. It is naturally expected that the coexistence of both charge and spin ordering may lead to nonlinear optical polarization $\mathbf{P}(2\omega)=\mathbf{P}^{FE}(2\omega)+\mathbf{P}^{AFM}(2\omega)$, which depends on two order parameters. In hexagonal $YMnO_3$, recent experiments[5] showed unambiguously the existence of two types of second harmonic spectra produced by a ferroelectric (noncentrosymmetric) ordering of charges and an antiferromagnetic (centrosymmetric) ordering of spins, respectively. Both the SHG's are of the electric-dipole character, but have different symmetries with respect to time-space inversion symmetry operations. An interference phenomenon between the two nonlinear optical fields has also been observed and used to visualize the 180° antiferromagnetic domains that exist below the Neel temperature T_N, which could not be distinguished in linear optics.[5] Although the experimental observations have been explained by a phenomenological model based on the crystallographic and magnetic symmetries of $YMnO_3$, it is still important to develop a microscopic theory for the nonlinear optical spectroscopy due to the coexistence of the two order parameters in $YMnO_3$, taking into account the structural, magnetic, and electric properties of hexagonal $YMnO_3$. This kind of theory will be helpful in understanding the physical origin of the colossal magnetoresistance.

The multiband Hubbard Hamiltonian has been very successful in describing a strongly correlated electronic system, and widely used to study the electronic and magnetic structures in superconducting oxides, transition-metal oxides, and colossal magnetoresistance material.[9–12] Since exact analytic solutions of the Hubbard model cannot be obtained in two and three dimensions, one usually employs certain approximations. The unrestricted Hartree-Fock (HF) approximation is one of the most straightforward and well-defined approximations. It correctly produces the major feature of d bands in the presence of strong electron-electron interaction. An unrestricted HF approximation has been successfully used in transition-metal oxides.[13] The same approximation was also applied recently by Mizokawa and Fujimori to study the interplay between charge, spin, and orbital orderings systematically in a series of perovskite-type $3d$ transition-metal

oxides.[14] Their results were very encouraging, and they found that the unrestricted HF method generally yields a qualitatively correct description of the electronic and magnetic properties of perovskite oxides in comparison with experimental observation.[14] The validity of the unrestricted HF approach to Mott insulators was generally discussed a long time ago by Brandow,[15] who concluded that an unrestricted HF calculation of the Hubbard model gives a useful picture of metallic versus insulating behavior of $3d$ transition-metal oxides. As is well known, the HF method gives a qualitatively correct result in the first-order approximation, and better methods such as the slave boson method may change the result quantitatively but not qualitatively. Thus, in this paper, based upon the multiband Hubbard Hamiltonian and the unrestricted Hartree-Fock approximation, we try to use the real-space recursion method to calculate the electronic structure of $YMnO_3$ below T_N, and then develop a method to calculate its nonlinear optical susceptibility. The calculated results will be compared with the experimental observations, identifying the different contributions to the optical susceptibility from the antiferromagnetic and ferroelectric orders, respectively.

Many physical models have been proposed to calculate the nonlinear optical susceptibilities of materials[16] since the pioneering work of Bloembergen. Rojo and Mahan used the Lanczos method to calculate the static hyperpolarizability of polymers.[17] Using the self-consistent Sternheimer method, Johnson, Subbaswamy and Senatore calculated the static linear and nonlinear polarizabilities of alkali halides.[18,19] There are still some other methods to calculate linear and nonlinear polarizabilities of materials. The first one uses time-dependent perturbation theory to find a solution of the Schrödinger equation, which is usually called the sum-over-state method.[20] The other one uses the density-matrix formalism to give the static and dynamic optical susceptibilities.[21] These two methods are usually done in momentum and energy spaces. All of them need to know the eigenvalues and eigenfunctions of the system, and so could not be used in larger cluster systems and disordered systems. Since the optical property is a rather localized effect arising from the interaction between incident photons and electrons in the orbitals of a certain cluster,[22] in this paper we prefer to study the nonlinear optical properties of $YMnO_3$ by using time-dependent perturbation theory to derive an expression of the second-order nonlinear optical susceptibility in terms of the real-space Green's function, which can be easily obtained by the recursion method and other real-space calculation techniques. The real-space recursion method is a powerful numerical technique to obtain spectral properties of any operator, and can be used to solve a wide range of problems, from identifying the relative stability of a transition-metal alloy structure to obtaining the electronic and topological structures of amorphous semiconductors. It has more advantages in applications to larger clusters, systems with lower symmetry, disordered systems, or periodical systems having complex unit cells.[23] Previously, the recursion method was used mainly to calculate the density of states and total energy of a system.

The rest of the paper is organized as follows: In Sec. II, we introduce the multiband Hubbard model and the unrestricted Hartree-Fock approximation; then we derive an expression for the nonlinear optical susceptibility in terms of the real-space Green's function. In Sec. III. we present numerical results and a discussion. Conclusions are drawn in Sec. IV.

II. MODEL HAMILTONIAN AND FORMULATION

Following Mizokawa and Fujimori, we used a multiband Hubbard model, which includes a tenfold degeneracy of the transition-metal $3d$ orbitals and a sixfold degeneracy of the oxygen $2p$ orbitals, as well as on-site Coulomb and exchange interaction[14]:

$$H = H_0 + H_1,$$

$$\begin{aligned} H_0 = & \sum_{im\sigma} \epsilon^0_{dm} d^\dagger_{im\sigma} d_{im\sigma} + \sum_{jn\sigma} \epsilon_p p^\dagger_{jn\sigma} p_{jn\sigma} \\ & + \sum_{ijmn\sigma} (t^{mn}_{ij} d^\dagger_{im\sigma} p_{jn\sigma} + \text{H.c.}) \\ & + \sum_{ijnn'\sigma} (t^{nn'}_{ij} p^\dagger_{in\sigma} p_{jn'\sigma} + \text{H.c.}), \end{aligned} \tag{1}$$

$$\begin{aligned} H_1 = & \sum_{im} u d^\dagger_{im\uparrow} d_{im\uparrow} d^\dagger_{im\downarrow} d_{im\downarrow} \\ & + \frac{1}{2} \sum_{im \neq n\sigma\sigma'} u' d^\dagger_{im\sigma} d_{im\sigma} d^\dagger_{in\sigma'} d_{in\sigma'} \\ & - j \sum_{im\sigma\sigma'} d^\dagger_{im\sigma} \vec{\sigma} d_{im\sigma'} \mathbf{S}^d_{im}, \end{aligned}$$

where $d_{im\sigma}(d^\dagger_{im\sigma})$ and $p_{jn\sigma}(p^\dagger_{jn\sigma})$ denote the annihilation (creation) operators of an electron on Mn $3d$ orbitals at site i and O $2p$ orbitals at site j, respectively; m and n are the orbital indices and σ the spin index. ϵ^0_{dm} and ϵ_p are their corresponding on-site energies, and ϵ^0_{dm} includes the crystal-field splitting energy, i.e., $\epsilon^0_d(t_{2g}) = \epsilon^0_d - 4$ Dq and $\epsilon^0_d(e_g) = \epsilon^0_d + 6$ Dq, with ϵ^0_d the bare on-site energy of the $3d$ orbitals. t^{mn}_{ij} and $t^{nn'}_{ij}$ are the nearest-neighbor $2p$-$3d$ and $2p$-$2p$ hopping integrals which are expressed in terms of Slater-Koster parameters $pd\sigma$, $pd\pi$, $pp\sigma$, and $pp\pi$.[24] S^d_{im} is the total spin operator of a Mn ion, extracting the spin operator in the orbital m. $u' = u - \frac{5}{2}j$, and the parameter u is related to the multiplet averaged d-d Coulomb interaction U via $u = U + \frac{20}{9}j$.

In the unrestricted Hartree-Fock approximation, the mean-field Hamiltonian becomes

$$\begin{aligned} H^{HF} = & \sum_{im\sigma} \Big[\epsilon^0_{dm} + u n^d_{im\bar{\sigma}} - \frac{j}{2} \sigma (\mu^d_t - \mu^d_m) \\ & + u' (n^d_t - n^d_m) \Big] d^\dagger_{im\sigma} d_{im\sigma} + \sum_{jn\sigma} \epsilon_p p^\dagger_{jn\sigma} p_{jn\sigma} \\ & + \sum_{ijmn\sigma} (t^{mn}_{ij} d^\dagger_{im\sigma} p_{jn\sigma} + \text{H.c.}) + \sum_{ijn'n\sigma} (t^{nn'}_{ij} p^\dagger_{in\sigma} p_{jn'\sigma} \\ & + \text{H.c.}) \end{aligned} \tag{2}$$

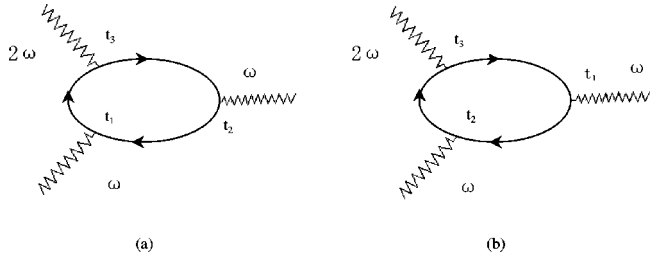

FIG. 1. The Feynman diagram for $\chi^{(2)}(-2\omega;\omega,\omega)$

Here n_t^d and μ_t^d are the total electron numbers and magnetization of the Mn $3d$ orbitals, respectively. They are defined as $n_t^d=\Sigma_{ms}n_{ms}^d$ with $n_{ms}^d=\langle d_{ms}^\dagger d_{ms}\rangle$, and $\mu_t^d=\Sigma_m\mu_m^d$ with $\mu_m^d=n_{m\uparrow}^d-n_{m\downarrow}^d$.

Using the recursion method, the real-space Green's function can be calculated in terms of a continued fraction,[23] and the multiband terminator is chosen in our calculation to close the continuous fractional.[25] Then the nonlinear optical susceptibility can be obtained by the calculated Green's function, and our derived expression for it.

Now we try to use the usual time-dependent perturbation theory in the interaction representation[26] and Feynman's diagrammatic rules to derive an expression for the optical susceptibility by the real-space Green's function.

The incoming and outgoing states are connected by the S matrix:

$$\Phi(+\infty)=S\Phi(-\infty), \tag{3}$$

$$S=T\exp\left[-i\int_{-\infty}^{+\infty}H'(t)dt\right], \tag{4}$$

$$H'=eE\Sigma r_i \tag{5}$$

The perturbing Hamiltonian (5) is the electric-dipole interaction. The second-order nonlinear optical susceptibility $\chi^{(2)}(-2\omega;\omega,\omega)$ is described as usual by connected Feynman diagrams composed of two incoming photon lines with energy ω, one outgoing line with energy 2ω, and a single-electron loop as in Fig. 1. The electron propagator is given by

$$K(2,1)=\begin{cases}-\dfrac{1}{\pi}\displaystyle\int_{E_f}^{\infty}dE\ \mathrm{Im}\ G_{12}(E)e^{-iE(t_2-t_1)}, & t_2>t_1\\ \dfrac{1}{\pi}\displaystyle\int_{-\infty}^{E_f}dE\ \mathrm{Im}\ G_{12}(E)e^{-iE(t_2-t_1)}, & t_2<t_1.\end{cases}$$

Here, $\mathrm{Im}\ G_{i,j}(\mathbf{E})=-\pi\Sigma_n\phi_n^*(\mathbf{r}_i)\phi_n(\mathbf{r}_j)\delta(\mathbf{E}-\mathbf{E}_n)$. Instead of integrating over the interaction times t_1, t_2, and t_3 independently, we consider all possible orderings of these and complete the integrals with respect to the relative times as in the proof of Goldstone's theorem.[26] One component of $\chi^{(2)}$, represented in Fig. 1(a) with an order of times $t_3>t_1>t_2$, is equal to

$$\int_{-\infty}^{E_f}d\varepsilon_g\int_{E_f}^{\infty}d\varepsilon_a\int_{E_f}^{\infty}d\varepsilon_b\frac{\mu}{(\epsilon_{ag}+\omega)(\epsilon_{bg}+2\omega)}. \tag{6}$$

For the same Fig. 1(a), but with an order of times, $t_1>t_2>t_3$, or $t_2>t_3>t_1$, we can obtain another two components of $\chi^{(2)}$, which are written as

$$\int_{-\infty}^{E_f}d\varepsilon_g\int_{E_f}^{\infty}d\varepsilon_a\int_{E_f}^{\infty}d\varepsilon_b\left[\frac{\mu}{(\epsilon_{ag}-2\omega)(\epsilon_{bg}-\omega)}+\frac{\mu}{(\epsilon_{ag}+\omega)(\epsilon_{bg}-\omega)}\right]. \tag{7}$$

Similarly, for Fig. 1(b), with all different orders of times, we obtain their contributions to $\chi^{(2)}$ as

$$-\int_{-\infty}^{E_f}d\varepsilon_g\int_{E_f}^{\infty}d\varepsilon_a\int_{-\infty}^{E_f}d\varepsilon_b\left[\frac{\mu}{(\epsilon_{ag}+\omega)(\epsilon_{ab}+2\omega)}+\frac{\mu}{(\epsilon_{ag}-2\omega)(\epsilon_{ab}-\omega)}+\frac{\mu}{(\epsilon_{ag}+\omega)(\epsilon_{ab}-\omega)}\right]. \tag{8}$$

Here μ is defined as

$$\mu=\sum_i\sum_j\sum_k\ \mathrm{Im}\ G_{i,j}(\varepsilon_g)\mathrm{Im}\ G_{k,i}(\varepsilon_a)\mathrm{Im}\ G_{j,k}(\varepsilon_b)\mathbf{r}_i\mathbf{r}_j\mathbf{r}_k.$$

In the above formula, $\epsilon_{ag}=\epsilon_a-\epsilon_g$, and $\epsilon_a(\epsilon_g)$ is one-electron energy. E_f is the Fermi energy. Equations (6)–(8) are our basic equations used to calculate $\chi^{(2)}(-2\omega;\omega,\omega)$ for $YMnO_3$.

III. CALCULATED RESULTS AND DISCUSSIONS

The band-structure parameters used in our numerical calculations are obtained by fitting the cluster-model photoemission spectra of the valence band and the transition-metal $2p$ core level to experimental spectra.[27] In this paper, the bare on-site energies of Mn $3d$ and O $2p$ orbitals are taken as $\epsilon_d^0=-25.5$ eV and $\epsilon_p=0$ eV. The crystal-field splitting energy and the Slater-Koster parameters are chosen as 10 Dq $=1$ eV, and $pd\sigma=-1.8$ eV, $pd\pi=0.9$ eV, $pp\sigma=0.6$ eV, and $pp\pi=-0.15$ eV, respectively. The on-site Coulomb repulsion energy and Hund coupling constant are taken as $U=7.5$ eV and $j=0.76$ eV. With the set of parameters given above, we calculated the electronic structures of $YMnO_3$ self-consistently by the iteration scheme. Its density of states in the energy range of -12 eV to 8 eV is shown in Fig. 2. For convenience, the Fermi energy ($E_f=0$) is set at the middle of the band gap, which is 1.48 eV. The top panel represents the total density of states of $YMnO_3$, and the middle and bottom panels are the partial densities of states for Mn $3d$ and O $2p$ orbitals, respectively. As can be seen from Figs. 2(b)–2(d), the main contributions to the density of states near the Fermi energy are given by the Mn e_g and O p orbitals. The electron occupation numbers in the t_{2g} and e_g bands are 3.098 and 1.406, respectively. The extra electrons in the Mn $3d$ band come from O $2p$ orbitals due to the hybridization between them. The magnetic moment on Mn ion is $3.7\mu_B$, which is larger than the experimental value $3.1\mu_B$.[28] The bandwidth of Mn t_{2g} orbitals is much narrower than the Mn e_g orbital, indicating that t_{2g} orbitals are more localized than the e_g orbital.

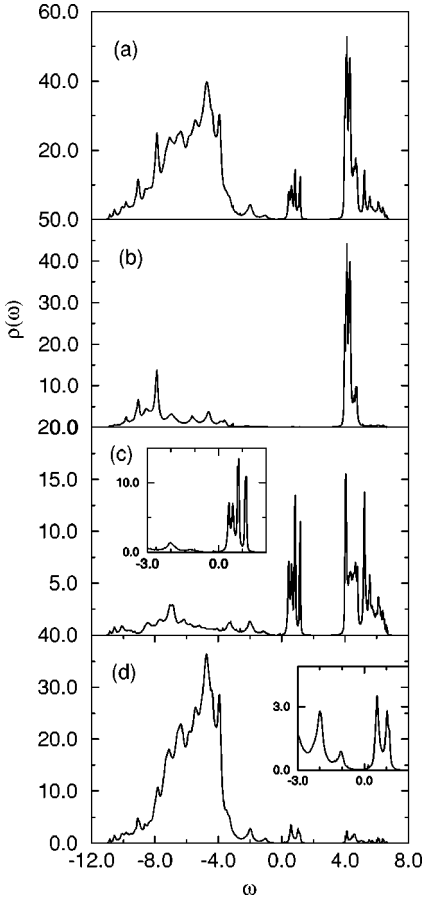

FIG. 2. Density of states of hexagonal $YMnO_3$. The unit of the x coordinate is eV. (a) Total density of states (b), (c), and (d) Partial densities of states for Mn t_{2g}, Mn e_g, and O p bands, respectively.

Hexagonal $YMnO_3$ belongs to the noncentrosymmetric $P6_3cm$ space group. Below T_c its SHG can be produced by electric dipoles due to the ferroelectric ordering of the charge. Based upon group theory, it is known that there are only four independent tensor elements of the second-order nonlinear optical susceptibility ($\chi_{xzx}=\chi_{yzy}$, $\chi_{xxz}=\chi_{yyz}$, $\chi_{zxx}=\chi_{zyy}$, and χ_{zzz}) due to its space structure symmetry.[16] Below T_N, hexagonal $YMnO_3$ belongs to the magnetic point group $\underline{6}m\underline{m}$, where spin ordering is centrosymmetric,[29] which cannot contribute to $\chi^{(2)}$ by itself. However, the coexistence of antiferromagnetic ordering with ferroelectric ordering in $YMnO_3$ gives rise to an electric-dipole susceptibility χ_{xxx}.[5] χ_{zzz}, χ_{zxx}, and χ_{xxx} are calculated based upon Eqs. (6)–(8). Their static values are 11.7, 2.89 and 1.91 $\times 10^{-8}$ esu, respectively. Static χ_{zzz} is the largest, and both static χ_{zzz} and χ_{zxx} are larger than static χ_{xxx}, probably because both of χ_{zxx} and χ_{zzz} stem directly from the electric dipole contribution; however χ_{xxx} is magnetization induced, and therefore is an indirect electric dipole contribution.

Fröhlich et al. measured the SH spectra of $YMnO_3$ in the energy range $2\hbar\omega=2.0-3.2$ eV at $T=6$ K. They found that crystallographic-induced χ_{zxx} has a peak located at $2\omega=2.7$ eV, and antiferromagnetic-induced χ_{xxx} has a peak at $2\omega=2.46$ eV.[5] In order to compare with experiment, we have also investigated the dynamic optical response of $YMnO_3$. Dispersions of χ_{xxx}, χ_{zxx}, and χ_{zzz} are calculated and shown in Fig. 3. Positions of the first peak are located at

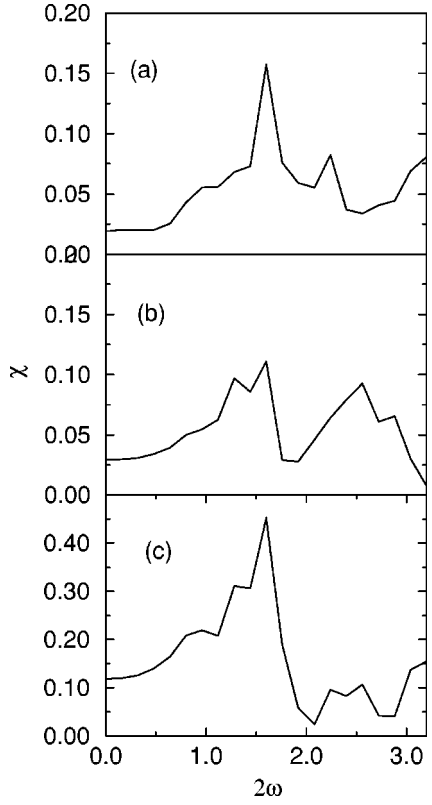

FIG. 3. The dynamical response of the second-order nonlinear optical susceptibity for hexagonal $YMnO_3$ (in 10^{-6} esu). The unit of the x coordinate is eV. (a) χ_{xxx}. (b) χ_{zxx}. (c) χ_{zzz}.

$2\omega=1.6$, 1.28, and 0.96 eV for χ_{xxx}, χ_{zxx}, and χ_{zzz}, with peak values, 1.572, 0.970 and 2.192 $\times 10^{-7}$ esu, respectively. The highest peaks of χ_{xxx}, χ_{zxx}, and χ_{zzz} are located at the same $2\omega=1.6$ eV, and their values are 1.572, 1.108, and 4.517 $\times 10^{-7}$ esu, respectively. It can be seen from Fig. 3 that there is one peak of χ_{xxx} located at $2\omega=2.24$ eV in the energy range of 2.0–3.0 eV. The peak value is 8.214 $\times 10^{-8}$ esu. In the same range, there are two peaks in χ_{zxx} located at $2\omega=2.60$ and 2.88 eV, and their values are 9.257 and 6.538×10^{-8} esu, respectively. It is obvious that in general our calculated peak positions are very consistent with the experimental data, and only the position of the calculated χ_{xxx} peak shifts slightly to lower energy than that of the experimental value (the theoretical value of $2\omega=2.24$ eV versus the experimental one of $2\omega=2.46$ eV).[5]

The complete band structure of Mn d and O p contains many band branches, which are responsible for different regions of the $\chi^{(2)}$ spectra. The experimental frequency range $2\hbar\omega=2.0$–3.2 eV involves only bands around the Fermi surface. From Fig. 2, we can see there are no Mn t_{2g} states near the Fermi surface. Therefore, only the Mn e_g and O p bands makes contributions to the low-frequency components of χ_{zxx} and χ_{xxx} spectra observed in the experiment. From the inset of Figs. 2(c) and 2(d), we can see the peaks in the density of states (DOS) of the Mn e_g band are located at -2.02, -1.18, 0.44, 0.60, 0.80, 0.85, 1.13, and 1.16 eV. The peaks in the DOS of the O p band are located at -1.99, -1.04, 0.58, and 1.16 eV. Hence both the 2.24-eV peak in the χ_{xxx} spectra and the 2.6-eV peak in the χ_{zxx} spectra are two-photon resonance peaks, and are caused by transitions

between the Mn e_g band to the Mn e_g band, the Mn e_g band to the O p band, and the O p band to the O p band. Since our calculation has been done in real space, it is very easy to decide the ratio between the three different contributions. We find the contribution from the transition between O p and O p bands is the lowest. Also, the contributions from the transitions of Mn e_g to Mn e_g and Op to Mn e_g bands are about equal to each other in magnitude (the ratio of the former to the latter is about 0.45 to 0.55), indicating that the effect of the latter cannot be neglected, which is different from the simple explanation for the resonance peaks in $\chi^{(2)}$ in $YMnO_3$ from the phenomenological model based only upon the symmetries of the system.

There are two peaks in χ_{zzz} spectra in the range from 2.0 to 3.0 eV. Their positions are $2\omega=2.24$ and 2.60 eV, and their values are 0.954 and 1.067×10^{-7} esu, which are larger than that of χ_{zxx}. It will be more interesting to measure their values.

In order to see how the Coulomb interaction affects the $\chi^{(2)}$ spectra, we have also calculated χ_{xxx}, χ_{zxx}, and χ_{zzz} of $YMnO_3$ with different U's. We find that the influence of Coulomb interaction on the nonlinear optical property of $YMnO_3$ is similar to that in carbon nanotubes.[30] We find that with an increase of U, χ_{xxx}, χ_{zxx}, and χ_{zzz} will decrease, and the peak positions in their spectra will shift to right, i.e., to higher frequencies, because an increasing Coulomb interaction U will increase the energy gap.

IV. CONCLUSION

In this paper, we present an expression for the second-order nonlinear optical susceptibility in terms of the real-space Green's function, which is calculated by the recursion method. Then, using our derived formula, we investigate the nonlinear optical properties of $YMnO_3$, and find that peaks of low frequency in $\chi^{(2)}$ are caused mainly by transitions of Mn e_g to Mn e_g bands, and Mn e_g to O p bands, indicating the importance of the latter. Our main result is in agreement with the experiment. Our method can be applicable to many other systems (for example, clusters, systems with complex unit cells, and disorder systems). There are many methods which can be used to calculate the real-space Green's function. This, using our derived expressions, all these methods can be used to calculate the nonlinear optical susceptibility.

ACKNOWLEDGMENTS

The authors acknowledge support in this work by a grant for State Key Program of China, and support from the National Science Foundation of China through Grant No. 19677202. The numerical calculations in this work were made on the SGI Origin–2000 computer in the Group of Computational Condensed Matter Physics, National Laboratory of Solid State Microstructures, Nanjing University.

[1] S. Jin, T.H. Tiefel, M. McCormack, R.A. Fastnact, R. Ramesh, and L.H. Chen, Science **264**, 413 (1994); R. von Helmolt, J. Wecker, B. Holzapfel, L. Schultz, and K. Samwer, Phys. Rev. Lett. **71**, 2331 (1993).

[2] F. Bertant, F. Forrat, and P. Fang, C.R. Acad. Sci. URSS **256**, 1958 (1963); H.L. Yakel, W.C. Koehler, E.F. Bertant, and E.F. Forrat, Acta Crystallogr. **16**, 957 (1963).

[3] Z.J. Huang, Y. Cao, Y.Y. Sun, Y.Y. Xue, and C.W. Chu, Phys. Rev. B **56**, 2623 (1997).

[4] M. Fiebig, D. Fröhlich, B.B. Krichevtsov, and R.V. Pisarev, Phys. Rev. Lett., **73**, 2127 (1994).

[5] D. Fröhlich, St. Leute, V.V. Pavlov, and R.V. Pisarev, Phys. Rev. Lett. **81**, 3239 (1998).

[6] J. Reif, J.C. Zink, C.M. Schneider, and J. Kirschner, Phys. Rev. Lett. **67**, 2878 (1991); J. Reif, C. Rau, and E. Matthias, *ibid.* **71**, 1931 (1993).

[7] B. Koopmans, M. Groot Koerkamp, Th. Rasing, and H. Van den Berg, Phys. Rev. Lett. **74**, 3692 (1995); M. Straub, R. Vollmer, and J. Kirschner, *ibid.* **77**, 743 (1996).

[8] V.V. Pavlov, R.V. Pisarev, A. Kirilyuk, and Th. Rasing, Phys. Rev. Lett. **78**, 2004 (1997).

[9] V.J. Emery, Phys. Rev. Lett. **58**, 2794 (1987); P.W. Anderson, Science **235**, 1196 (1987); P.W. Anderson, G. Baskaran, Z. Zou, and T. Hsu, Phys. Rev. Lett. **58**, 2790 (1987).

[10] N.F. Mott, Proc. Phys. Soc., London, Sect. A **62**, 416 (1949).

[11] J. Hubbard, Proc. R. Soc. London, Ser. A **276**, 238 (1963); **277**, 237 (1964); **281**, 401 (1964).

[12] J. Inoue and S. Maekawa, Phys. Rev. Lett. **74**, 3407 (1995).

[13] C. Castellani, C.R. Natoli, and J. Ranninger, Phys. Rev. B **18**, 4945 (1978); J. Ashkenazi and M. Weger, Adv. Phys. **22**, 207 (1973).

[14] T. Mizokawa and A. Fujimori, Phys. Rev. B **53**, R4201 (1996); **54**, 5368 (1996); **51**, 12 880 (1995).

[15] B.H. Brandow, Adv. Phys. **26**, 651 (1977).

[16] N. Bloembergen, *Nonlinear Optics* (Benjamin, New York, 1965); Y. R. Shen, *The Principles of Nonlinear Optics* (Wiley, New York, 1984).

[17] A.G. Rojo and G.D. Mahan, Phys. Rev. B **47**, 1794 (1993); G.D. Mahan and A.G. Rojo, *ibid.* **50**, 2642 (1994).

[18] M.D. Johnson, K.R. Subbaswamy, and G. Senatore, Phys. Rev. B **36**, 9202 (1987); **37**, 6508 (1988).

[19] M.D. Johnson and K.R. Subbaswamy, Phys. Rev. B **39**, 10 275 (1989).

[20] B.J. Orr and J.F. Ward, Mol. Phys. **20**, 513 (1971); J. Yu and W.P. Su, Phys. Rev. B **44**, 13 315 (1991).

[21] S. Mukamel, A. Takahashi, H.X. Wang, and G. Chen, Science **266**, 250 (1994); J.E. Sipe and Ed Ghahramani, Phys. Rev. B **48**, 11 705 (1993).

[22] C.T. Chen, Y. Wu, A. Jiang, B. Wu, G. You, R. Li, and S. Lin, J. Opt. Soc. Am. B **6**, 616 (1989); R.H. French, J.W. Ling, F.S. Ohuchi, and C.T. Chen, Phys. Rev. B **44**, 8496 (1991).

[23] V. Heine, R. Haydock, and M. J. Kelly, in *Solid State Physics, Advances in Research and Applications*, edited by H. Ehrenreich, F. Seitz, and D. Turnbull (Academic, New York, 1980) Vol. 35, p. 215.

[24] J.C. Slater and G.F. Koster, Phys. Rev. **94**, 1498 (1954).

[25] R. Haydock and C.M.M. Nex, J. Phys. C **17**, 4783 (1984).

[26] A. L. Fetter and J. D. Walecka, *Quantum Theory of Many-Particle Systems* (McGraw-Hill, New York, 1971); J. J. Sakurai,

Advanced Quantum Mechanics (Cummings, Menlo Park, 1984).
[27] A.E. Bocquet, T. Mizokawa, T. Saitoh, H. Namatama, and A. Fujimori, Phys. Rev. B **46**, 3771 (1992).
[28] Numerical Data and Functional Relationships, edited by K. H. Hellwege and A. M. Hellwege, Landolt-Bornstein, New Series, Group III, Vol. 16, Pt. a. (Springer-Verlag, Berlin, 1981).
[29] W. Sikora and V.N. Syromyatnikov, J. Magn. Magn. Mater. **60**, 199 (1986).
[30] X. Wan, J. Dong, and D.Y. Xing, Phys. Rev. B **58**, 6756 (1998).